A Succinct Explicit Local Time-Stepping Method for Helmholtz Wave Equation Based Discontinuous Galerkin Time Domain Method for 3-D Multiscale Electromagnetic Modeling

Peng Wang and Yan Shi

School of Electronic Engineering
Xidian University, Xi'an, 710071, China
15029038715@163.com and shiyan@mail.xidian.edu.cn

Abstract ─ A succinct explicit local time-stepping (LTS) method for Helmholtz wave equation based discontinue Galerkin time domain method has been developed to analyze 3-D multiscale electromagnetic problems. In the proposed LTS scheme, a simple linear interpolation procedure is implemented to calculate the fields in the subdomain with the larger mesh size at the time steps corresponding to its neighboring subdomains with the smaller mesh size, and thus the proposed method can be easily generalized to the situation of the multiple subdomains with arbitrary time step ratio. With the proposed LTS method, the computational efficiency can be improved for the analysis of the multiscale problems. Several numerical examples including dielectric loaded resonance cavity, microstrip filter, and Vivaldi antenna are given to illustrate good performance of the proposed succinct explicit LTS method.

Index Terms ─ Arbitrary integral time step ratio, discontinue Galerkin time domain, local time-stepping (LTS), multiple subdomains, vector wave equation.

I. INTRODUCTION

In recent years, the discontinuous Galerkin time-domain (DGTD) methods have been rapidly developed for transient simulation of electromagnetic problems [1-5]. Compared with the conventional finite difference time domain (FDTD) method [6], the DGTD method can model the complex structures easily and obtain higher-order solution accuracy. With the use of numerical fluxes defined on the interface between two adjacent elements and explicit time integration method [1-5], the DGTD methods can lead to block-diagonal mass matrices with the block size equal to the number of degrees of freedom per element, thus leading to a highly efficient parallel solution scheme.

The conventional DGTD method is based on the Maxwell equations, which needs to solve the electric field **E** and the magnetic field **H** simultaneously. On the other hand, due to the use of the numerical flux, the conventional DGTD method results in more degrees of freedom, which consumes more computational resources. Recently, an interior penalty discontinuous Galerkin time domain (IPDG-WE) method has been developed to solve the complicate EM problems. Built on the Helmholtz wave equation, the IPDG-WE method [7, 8] only needs to solve one field variable, which can achieve significant reduction in computational time and memory usage. Moreover, with the introduction of the interior penalty fluxes, the IPDG-WE method can achieve optimal convergence rate of $O(h^{p+1})$ and meanwhile be free from the numerical dissipation, which the conventional DGTD method suffers from [7, 8].

The real-life electromagnetic problems generally involve various complex objects with multiscale geometries. When modelling this kind of the objects, the sizes of the discretization meshes are significantly different. With either the DGTD or the IPDG-WE methods for the analysis of the multiscale problems, the time step must be chosen according to the smallest grid size in the computational domain due to the CFL stability of the explicit time integration scheme, thus resulting in a high computational cost. To overcome this stability restriction, the implicit time integration methods [9] and marching-on-in degree-based approaches [10-12] have been developed. However, these methods suffer from the larger memory consumption. Except implicit-like time integration methods, some explicit local time-stepping (LTS) schemes [13-17] have been proposed. By implementing the different time steps in the elements with the larger and smaller sizes, respectively, the computational efficiency can be improved. However, most of the local LTS schemes are based on the DGTD method [13-16]. Recently, Diaz and Grote [17] theoretically studies the LTS methods for second-order scale wave equations. No reports have been given about the LTS method for the second order Helmholtz wave equation based discontinuous Galerkin time domain method to model the practical 3D electromagnetic (EM) problems.

Submitted On: December 31, 2018
Accepted On: May 7, 2019

In this paper, we propose a succinct explicit LTS method combining the central difference time marching scheme in the IPDG method to model the practical 3D multiscale EM problems. With a simple linear interpolation scheme, the proposed LTS method needs no additional memory usages and introduces slightly computational overhead at the subdomain interfaces. Hence the proposed approach is very suitable to the multiple subdomains with arbitrary geometry ratio. Some practical 3D EM problems are presented to illustrate the efficiency and potential of the proposed LTS method.

II. FORMULATIONS

In this section, the IPDG method is first introduced. Then the succinct explicit LTS scheme is developed.

A. IPDG method

Let Ω be a computational domain which is discretized by N nonoverlapping tetrahedrons and terminated by boundary Γ_b, including perfect electric conductor (PEC) surface Γ_{PEC}, perfect magnetic conductor (PMC) surface Γ_{PMC} and first-order absorbing boundary condition (ABC) surface Γ_{ABC}. So we have $\Gamma_b = \Gamma_{PEC} \cup \Gamma_{PMC} \cup \Gamma_{ABC}$. We denote $\Gamma = \partial\Omega$ as all the faces in Ω and $\Gamma = \Gamma_i \cup \Gamma_b$, in which Γ_i is defined as the interior faces.

To avoid the late-time drifting problem, the IPDG method starts from a modified Helmholtz wave equation, i.e.,

$$\nabla\times\left(\mu^{-1}\nabla\times\tilde{\mathbf{E}}\right)+\varepsilon\frac{\partial^2\tilde{\mathbf{E}}}{\partial t^2}+\sigma\frac{\partial\tilde{\mathbf{E}}}{\partial t}=-\frac{\partial\mathbf{J}_S}{\partial t}, \tag{1}$$

where $\tilde{\mathbf{E}}=\partial_t^{-1}\mathbf{E}$. Here ε and μ are the permittivity and permeability, respectively. The hierarchical vector basis functions $\mathbf{N}_{k,j}(\mathbf{r})$ [18] are used to expand $\tilde{\mathbf{E}}$ in (1) as:

$$\tilde{\mathbf{E}}=\sum_{j=0}^{N_E}e_j(t)\mathbf{N}_j(\mathbf{r}), \tag{2}$$

in which $e_j(t)$ is the time dependent expansion coefficient and N_E is the number of the vector basis functions. Applying the Galerkin's spatial testing procedure with $\mathbf{N}_i$ into (1), we can have:

$$\begin{aligned}&\int_\Omega\varepsilon\frac{\partial^2\tilde{\mathbf{E}}}{\partial t^2}\cdot\mathbf{N}_i d\mathbf{r}+\int_\Omega\sigma\frac{\partial\tilde{\mathbf{E}}}{\partial t}\cdot\mathbf{N}_i d\mathbf{r}+\\&\int_\Omega\nabla\times\left(\mu^{-1}\nabla\times\tilde{\mathbf{E}}\right)\cdot\mathbf{N}_i d\mathbf{r}=-\int_\Omega\frac{\partial\mathbf{J}_S}{\partial t}\cdot\mathbf{N}_i d\mathbf{r}.\end{aligned} \tag{3}$$

By using the vector calculus identities and Gauss's theorem to the term $\nabla\times\left(\mu^{-1}\nabla\times\tilde{\mathbf{E}}\right)$ in (3) and introducing numerical fluxes, we obtain a weak form as:

$$\begin{aligned}&\int_\Omega\varepsilon\frac{\partial^2\tilde{\mathbf{E}}}{\partial t^2}\cdot\mathbf{N}_i d\mathbf{r}+\int_\Omega\sigma\frac{\partial\tilde{\mathbf{E}}}{\partial t}\cdot\mathbf{N}_i d\mathbf{r}\\&+\int_\Omega\mu^{-1}\tilde{\mathbf{E}}\cdot\nabla\times\left(\nabla\times\mathbf{N}_i\right)d\mathbf{r}+\sum_{\Omega_K\in\Omega}\int_{\partial\Omega_K}\mathbf{n}\times\left(\mu^{-1}\tilde{\mathbf{E}}\right)^*\cdot\nabla\times\mathbf{N}_i dS\\&+\sum_{\Omega_K\in\Omega}\int_{\partial\Omega_K}\mathbf{n}\times\left(\mu^{-1}\nabla\times\tilde{\mathbf{E}}\right)^*\cdot\mathbf{N}_i dS=-\int_\Omega\frac{\partial\mathbf{J}_S}{\partial t}\cdot\mathbf{N}_i d\mathbf{r},\end{aligned} \tag{4}$$

in which superscript * denotes the numerical flux. Further, (4) is rewritten as a strong from, i.e.,

$$\begin{aligned}&\int_\Omega\varepsilon\frac{\partial^2\tilde{\mathbf{E}}}{\partial t^2}\cdot\mathbf{N}_i d\mathbf{r}+\int_\Omega\sigma\frac{\partial\tilde{\mathbf{E}}}{\partial t}\cdot\mathbf{N}_i d\mathbf{r}+\int_\Omega\mu^{-1}\nabla\times\tilde{\mathbf{E}}\cdot\nabla\times\mathbf{N}_i d\mathbf{r}+\\&\sum_{\Omega_K\in\Omega}\int_{\partial\Omega_K}\mathbf{n}\times\left(\tilde{\mathbf{E}}^*-\tilde{\mathbf{E}}\right)\cdot\mu^{-1}\nabla\times\mathbf{N}_i dS+\\&\sum_{\Omega_K\in\Omega}\int_{\partial\Omega_K}\mathbf{n}\times\left(\mu^{-1}\nabla\times\tilde{\mathbf{E}}\right)^*\cdot\mathbf{N}_i dS=-\int_\Omega\frac{\partial\mathbf{J}_S}{\partial t}\cdot\mathbf{N}_i d\mathbf{r}.\end{aligned} \tag{5}$$

The numerical fluxes are vital to the accuracy and stability of the IPDG method. The well-defined numerical fluxes can be obtained as [7, 8]:

$$\begin{aligned}\tilde{\mathbf{E}}^*&=\begin{cases}\left\{\tilde{\mathbf{E}}\right\} & f\subset\Gamma_i\\ 0 & f\subset\Gamma_{PEC}\\ \tilde{\mathbf{E}} & f\subset\Gamma_{PMC}\\ \tilde{\mathbf{E}} & f\subset\Gamma_{ABC}\end{cases},\\\left(\mu^{-1}\nabla\times\tilde{\mathbf{E}}\right)^*&=\begin{cases}\left\{\mu^{-1}\nabla\times\tilde{\mathbf{E}}\right\}-\tau_f\left[\!\left[\tilde{\mathbf{E}}\right]\!\right]_T & f\subset\Gamma_i\\ \mu^{-1}\nabla\times\tilde{\mathbf{E}}-\tau_f\tilde{\mathbf{E}} & f\subset\Gamma_{PEC}\\ 0 & f\subset\Gamma_{PMC}\\ -Y_s\mathbf{n}\times\mathbf{n}\times\partial\tilde{\mathbf{E}}/\partial t & f\subset\Gamma_{ABC}\end{cases},\end{aligned} \tag{6}$$

in which τ_f is an interior penalty parameter defined on the interface. The tangential jump $[\![\cdot]\!]_T$ and average $\{\cdot\}$ across an interface are expressed as,

$$\left[\!\left[\mathbf{u}\right]\!\right]_T=\begin{cases}\mathbf{n}^-\times\mathbf{u}^-+\mathbf{n}^+\times\mathbf{u}^+ & f\subset\Gamma_i\\ \mathbf{n}^-\times\mathbf{u}^- & f\subset\Gamma_b\end{cases}, \tag{7}$$

and,

$$\left\{\mathbf{u}\right\}=\begin{cases}\dfrac{\mathbf{u}^-+\mathbf{u}^+}{2} & f\subset\Gamma_i\\ \mathbf{u} & f\subset\Gamma_b\end{cases}. \tag{8}$$

Here the superscripts "-" and "+" denote the local element and the adjacent element corresponding to the face f, respectively.

By inserting (6) into (5), the semi-discrete system in each element yields:

$$\begin{aligned}&\left[\mathbf{M}_k\right]\left(\frac{\partial^2\tilde{\mathbf{e}}_k}{\partial t^2}\right)+\left[\mathbf{R}_k\right]\left(\frac{\partial\tilde{\mathbf{e}}_k}{\partial t}\right)+\left[\mathbf{S}_k^{mm}\right]\tilde{\mathbf{e}}_k\\&+\sum_f\left[\mathbf{S}_k^{mn,f}\right]\tilde{\mathbf{e}}_{k,f}=-\frac{\partial\tilde{\mathbf{j}}_k}{\partial t},\end{aligned} \tag{9}$$

in which $\tilde{\mathbf{e}}_k=[\tilde{e}_{k,1},\tilde{e}_{k,2},.....,\tilde{e}_{k,N_k}]_T$ denotes the vector of the expansion coefficients of the electric fields in the kth element, $\tilde{\mathbf{e}}_{k,f}$ denotes the coefficient vector in the elements adjacent to the kth element, and N_k is the number of the unknowns of the kth element. Here definitions of the matrices $\left[\mathbf{M}_k\right]$, $\left[\mathbf{R}_k\right]$, $\left[\mathbf{S}_k^{mm}\right]$ and $\left[\mathbf{S}_k^{mn,f}\right]$ can be found in [5].

Employing the central difference method to discretize

the time derivatives in (9) and sampling the electric fields at integer time steps $n\Delta t$ ($n = 0, 1, \ldots, N_t$), we can obtain the full-discrete system as

$$\begin{aligned}&\left(\left[\mathbf{M}_k\right]+\frac{\Delta t}{2}\left[\mathbf{R}_k\right]\right)\tilde{\mathbf{e}}_k^{n+1}=\\&\left(2\left[\mathbf{M}_k\right]+\Delta t^2\left[\mathbf{S}_k^{mm}\right]\right)\tilde{\mathbf{e}}_k^{n}-\Delta t^2\sum_f\left[\mathbf{S}_k^{mn,f}\right]\tilde{\mathbf{e}}_{k,f}^{n}\\&+\left(\frac{\Delta t}{2}\left[\mathbf{R}_k\right]-2\left[\mathbf{M}_k\right]\right)\tilde{\mathbf{e}}_k^{n-1}-\frac{\Delta t}{2}\left(\mathbf{j}_k^{n}-\mathbf{j}_k^{n-1}\right).\end{aligned}\tag{10}$$

B. Succinct explicit LTS method

In order to develop a multi-domain explicit LTS approach for the solution of the multiscale problem, we first consider the computational domain discretized by nonuniform meshes which can be categorized into two subdomains, as illustrated in Fig. 1. In each subdomain, the time step is chosen based on the minimal geometric sizes of the meshes according to CFL stability condition. Assume that ratio of the time steps in the two subdomains is p. Specifically, the time-steps in subdomains 1 and 2 are chosen as Δt_1 and $\Delta t_2=p\Delta t_1$, respectively. Let p an arbitrary positive integral number greater than 1 in this paper.

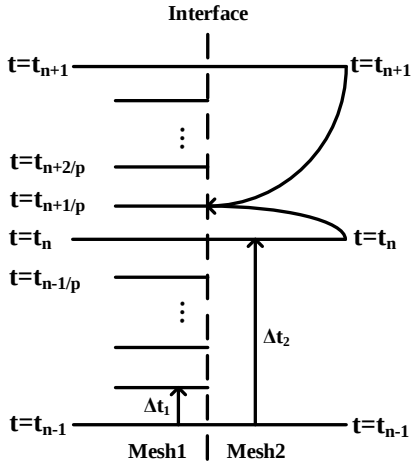

Fig. 1. The interface between two domains with the different meshes.

Consider that the subdomain 2 with the larger mesh size marches on from t_n to t_{n+1} in a time increment of Δt_2, while the subdomain 1 with the smaller mesh size successively marches on from t_n to t_{n+1} in a time increment of Δt_1. According to (10), we can know that the fields at the time step t_{n+1} in the elements of the subdomain 2 can be solved in the conventional way. On the other hand, the fields in the elements of the subdomain 1 except the elements adjacent to the interface between two subdomains are also updated in the traditional way. However, the fields at time step $t_{n+k/p}$ (k=2,3,⋯,p) in the elements on the interface of the subdomain 1 are solved in a modified way. In order to update the fields in an element of the subdomain 1 at time step $t_{n+k/p}$ (k=1,2,⋯,p-1), the fields of the subdomain 2 at the corresponding time step must be known. Here a linear interpolation approximation method is implemented to solve the fields in the subdomain 2 at the time step $t_{n+k/p}$ according to those at the time steps of t_n and t_{n+1}, i.e.,

$$\tilde{\mathbf{e}}^{n+k/p}=\left(1-\frac{k}{p}\right)\tilde{\mathbf{e}}^{n}+\left(\frac{k}{p}\right)\tilde{\mathbf{e}}^{n+1}.\tag{11}$$

Substituting (11) into (10), the fields in the element of the subdomain 1 at the time step $t_{n+(q+1)/p}$ can be solved as:

$$\begin{aligned}&\left(\left[\mathbf{M}_k\right]+\frac{\Delta t_1}{2}\left[\mathbf{R}_k\right]\right)\tilde{\mathbf{e}}_k^{n+(q+1)/p}\\&=\left(2\left[\mathbf{M}_k\right]+\Delta t_1^{\,2}\left[\mathbf{S}_k^{mm}\right]\right)\tilde{\mathbf{e}}_k^{n+q/p}-\Delta t_1^{\,2}\sum_{f\notin\text{interface}}\left[\mathbf{S}_k^{mn,f}\right]\tilde{\mathbf{e}}_{k,f}^{n+q/p}\\&-\Delta t_1^{\,2}\sum_{f\in\text{interface}}\left[\mathbf{S}_k^{mn,f}\right]\left(\left(1-\frac{q}{p}\right)\tilde{\mathbf{e}}_{k,f}^{n}+\left(\frac{q}{p}\right)\tilde{\mathbf{e}}_{k,f}^{n+1}\right)\\&+\left(\frac{\Delta t_1}{2}\left[\mathbf{R}_k\right]-2\left[\mathbf{M}_k\right]\right)\tilde{\mathbf{e}}_k^{n+(q-1)/p}-\frac{\Delta t_1}{2}\left(\mathbf{j}_k^{n+q/p}-\mathbf{j}_k^{n+(q-1)/p}\right).\end{aligned}\tag{12}$$

Comparing (12) and (10), we can find that in the proposed LTS-based scheme, no extra memory is required due to the use of the linear interpolation.

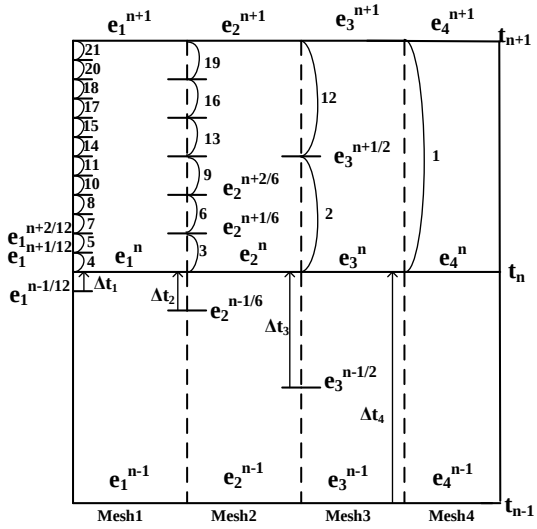

Fig. 2. The proposed LTS scheme for four subdomains with different meshes.

The proposed method can be easily generalized to the case of the multiple subdomains. Without the loss of generality, assume that there are four subdomains. The ratios of the mesh sizes in the four subdomains are 1: 2: 6: 12, as shown in Fig. 2. Therefore, the relationship of the time steps in the four subdomains becomes $\Delta t_4=2\Delta t_3=6\Delta t_2=12\Delta t_1$, where Δt_s (s=1,2,3,4) denotes the time step of the s-th subdomain.

Assume that all elements march on from the time step

t_n. The fields in the elements of the subdomain with the larger mesh size are first updated to its next time step, and then those with the smaller mesh size are stepped into the corresponding next time step successively. In this scenario, the linear interpolation method (11) can be implemented to solve the fields in the element of the subdomain with the larger mesh size at the time step corresponding to those of the subdomain with the smaller mesh size. And then (12) can be used to solve the fields in the elements of the subdomain with the smaller mesh size. It is worthwhile pointing out that the proposed LTS scheme can be applicable into the situation in which those elements adjacent to the certain element belong to more than two subdomains. Besides, in the proposed LTS method the arbitrary integral time step ratio between different subdomains can be valid.

In order to obtain a good speed up for the proposed LTS approach, a reasonably grouping strategy should be used. For a multiscale problem, the tetrahedrons with the different sizes are used to discretize the computational domain. All the tetrahedrons are first classified into different levels, i.e., Level=Int($10h/h_{\max}$), where h denotes the minimum edge length of each tetrahedron, h_{max} is the largest one among h, and Int (x) is a function to map a real number x to the largest integer not greater than x. Next, the tetrahedrons belonging to the neighboring levels are grouped into a subdomain according to the following criterions:

1. The number of the tetrahedrons which are adjacent to the interface between two subdomains is as small as possible;
2. The number of the tetrahedrons in the subdomain corresponding to the larger level is as many as possible;
3. The ratio of the time step between two neighboring subdomains is as large as possible.

It is worthwhile pointing out that we should use the above three criterions in a trade-off way to obtain a good speedup of the LTS method.

III. NUMERICAL RESULTS AND ANALYSIS

A. Dielectric ring in a resonant PEC cavity

As the first numerical example, a resonant PEC cavity with a dielectric ring shown in Fig. 3 is studied to demonstrate the accuracy and conservative energy property of the proposed method. The relative permittivity of the resonant ring is 2.06. The geometrical sizes of the computational region and the resonant ring are given in Fig. 3. The origin of coordinates is chosen as the center of the computational domain, and the center point of the resonant ring is set as (-45.25 mm, 0 mm, -21.5 mm). A dipole source is located at (-105 mm, -20 mm, 11.25 mm) and the observation point is chosen as (155 mm, 20 mm, 11.25 mm).

The computational region is meshed into some tetrahedrons with the average side length of λ/10 at 3 GHz, while the dielectric ring is discretized by using the refinement meshes with the average side length of λ/30 in order to get an accurate result. Therefore, there are 15,739 disjoint tetrahedrons in total and 3,463 tetrahedrons in the refinement region. In this example, all tetrahedrons are divided into ten different levels and are grouped into two subdomains. Ratio of the numbers of the discretized elements in two subdomains is shown as shown in Table 2. According to the CFL stability, the time steps of the two subdomains are chosen as 0.4×10^{-12} s and 1.6×10^{-12} s, respectively. A dipole source along the z-axis is used to generate a transient modulated Gaussian wave with a frequency band covering from 0.5 GHz to 5 GHz. Here the mixed 2nd order vector bases are adopted.

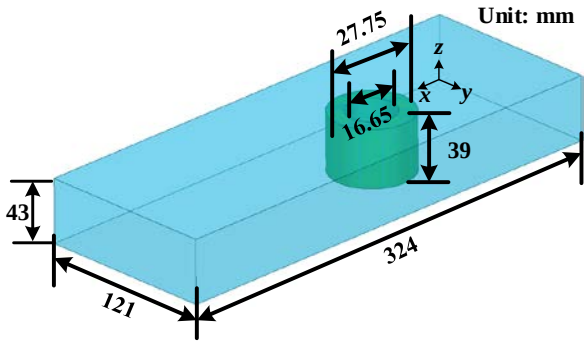

Fig. 3. Geometry of the resonant ring cavity.

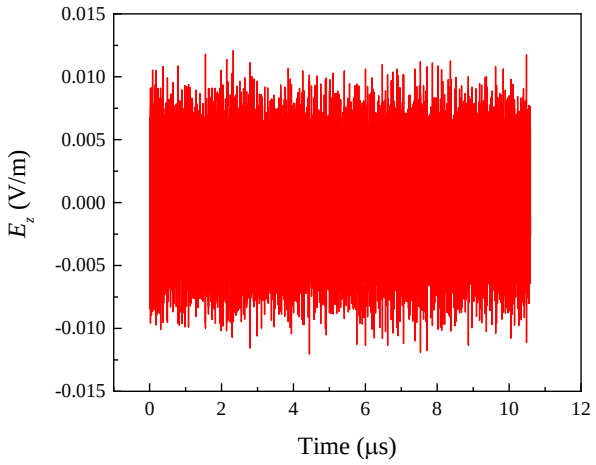

Fig. 4. Transient E_z component at the observation point.

The transient field E_z at the observation point is solved by the proposed method and plotted in Fig. 4. It can be seen from Fig. 4 that there is no numerical dissipation of the solution during a long simulation period more than 10 μs, and thus the proposed LTS-

based IPDG-WE method has energy conservation characteristic.

As shown in Table 1, the first eight resonance frequencies are extracted from the obtained time domain signals and compared with the results solved by the global time stepping (GTS) scheme and the high accuracy FDTD method [19]. The results by proposed LTS method agrees well with those by the GTS scheme and the in the reference. The computation performances of the LTS method and the GTS method are compared in Table 2. According to Table 2, the proposed LTS method can achieve 2.26 times speedup without the increase of the memory usage.

Table 1: The first eight resonant frequencies of the resonant PEC cavity, unit (GHz)

Scheme	FDTD	GTS	LTS
1st mode	1.2605	1.2503	1.2521
2nd mode	1.5076	1.5062	1.5061
3rd mode	1.8341	1.8303	1.8310
4th mode	2.1607	2.1564	2.1582
5th mode	2.5513	2.5431	2.5451
6th mode	2.6123	2.6092	2.6103
7th mode	2.8229	2.8213	2.8231
8th mode	3.0243	3.0202	3.0225

B. Microstrip filter

In the second example, a microstrip filter is analyzed by using the proposed method, as shown in Fig. 5. The relative permittivity of the substrate is 10.4 and the thickness is 1.27 mm. Two lumped ports are used in this example. The computational region terminated by the ABC boundary is set as 64 mm × 89.61 mm × 41.27 mm. The average size of the meshes in the whole region is chosen as $\lambda/10$ at 3 GHz and the regions corresponding to the narrow microstrip line are discretized by using the meshes with a higher spatial resolution. Hence, we have 52,948 tetrahedrons in total. The tetrahedrons are classified into ten different levels and then are grouped into 5 subdomains. Ratio of the mesh numbers in the 5 subdomains is 0.20:0.10:0.53:0.14:0.003, and therefore the time steps of the 5 subdomains are 0.28×10^{-13} s, 0.56×10^{-13} s, 1.12×10^{-13} s, 2.24×10^{-13} s and 4.48×10^{-13} s, respectively. The mixed 2nd order edge basis is used in this example. The S-parameters are calculated by the proposed LTS method and compared with the results by the GTS and FEM methods, as shown in Fig. 6. Good agreement between each other can be observed. Table 2 demonstrates comparison of the computational performance between the LTS and the GTS methods. The LTS method consumes less CPU time with the same memory usage.

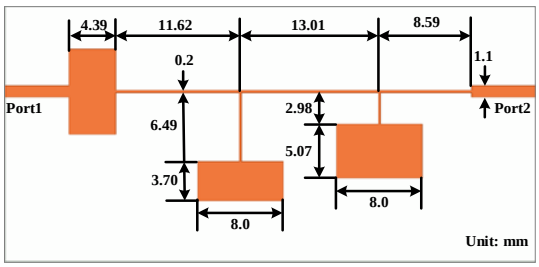

Fig. 5. Geometry of a microstrip filter.

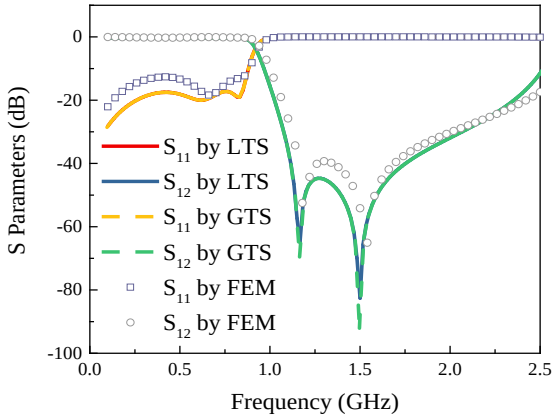

Fig. 6. S-parameters of the microstrip filter.

C. Vivaldi antenna

In the final example, a Vivaldi antenna is considered. The Vivaldi antenna is shown in Fig. 7, whose tapered slot is patterned with PEC ground plane on the top of the dielectric substrate. The relative permittivity of the substrate is 3.38 and the thickness is 1.524 mm. The geometrical parameters of the Vivaldi antenna are as follows: w_1 = 80 mm, w_2 = 0.5 mm, l_1 = 14.5 mm, l_2 = 12.9 mm, l_3 =12.6 mm, l_4 = 70 mm, l_5 = 3.2 mm, r =12 mm. The curves of the tapered slot are built by an exponential function of $e^{0.044x}$. One end of the slot is open to air and the other is ended with a circular slot. On the bottom of the substrate, there is a shorted 50 Ω microstrip feed line. A lumped port is used to excite the Vivaldi antenna.

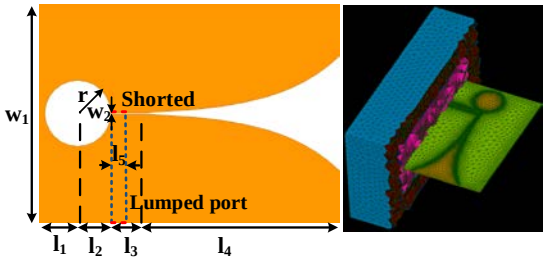

Fig. 7. Geometry and mesh of the Vivaldi antenna.

The computational domain is terminated by a perfectly matched layer (PML) which acts like an anechoic chamber absorbing all radiated energy. The whole region is meshed using a tetrahedral mesh with an approximate size length of 5 mm (λ/10 at 6 GHz), while the tapered slot is discretized by the meshes with the side length of 0.5 mm to guarantee the solution accuracy. The total number of the elements is 176895. Here 4 subdomains are used according to the side length of the tetrahedron, as shown in Table 2. The time step sizes of the 4 subdomains are set as 0.2×10^{-13} s, 0.8×10^{-13} s, 1.6×10^{-13} s and 3.2×10^{-13} s, respectively. Mixed 2nd order vector bases are utilized to expand the unknown fields. The S-parameter calculated by the proposed LTS method has a good agreement with those by the GTS and the FEM methods, as shown in Fig. 8. The performance comparison between the LTS and the GTS methods has been given in Table 2. A 6 times speedup is obtained by using the LTS-based method.

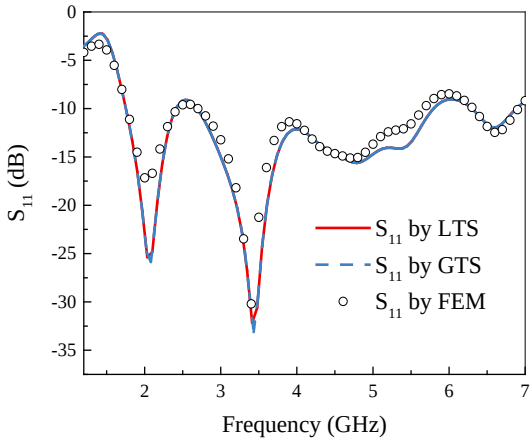

Fig. 8. S11 of the Vivaldi antenna.

Table 2: Performance comparison of LTS method and GTS method in the numerical examples

Examples	Method	Ratio of the Numbers of Elements in the Different Subdomains	Ratio of Time Steps in the Different Subdomains	Memory (MB)	Speedup Ratio
A	LTS	0.22: 0.78	1: 4	711	2.26
	GTS	------	------	711	
B	LTS	0.20: 0.10: 0.53: 0.14: 0.003	1: 2: 4: 8: 16	2332	2.23
	GTS	------	------	2332	
C	LTS	0.12: 0.26: 0.52: 0.10	1: 4: 8: 16	9988	6.00
	GTS	------	------	9988	

VI. CONCLUSION

In this paper, a succinct explicit LTS scheme for IPDG-WE method is presented to model 3-D multiscale electromagnetic problem. With a simple linear interpolation scheme, the proposed LTS method can be easily implemented in the situation of the multiple subdomains with arbitrary integral time step ratio. Good energy conservative property is achieved. Some numerical examples are given to illustrate good accuracy and speedup ratio without the increase of the memory usage for the solution of 3-D multiscale electromagnetic problems.

ACKNOWLEDGMENT

This work was supported by National Natural Science Foundation of China (No. 61771359), Natural Science Basic Research Plan in Shaanxi Province under Grant 2018JM6006, and Fundamental Research Funds for the Central Universities (No. JBF180202).

REFERENCES

[1] J. S. Hesthaven and T. Warburton, *Nodal Discontinuous Galerkin Methods: Algorithms, Analysis, and Applications*.Springer, New York, 2008.

[2] P. Wang, Y. Shi, C. Y. Tian, and L. Li, "Analysis of Graphene-based devices using wave equation-based discontinuous Galerkin time domain method," *IEEE Antennas and Wireless Propagation Letters*, vol. 17, no. 12, pp. 2169-2173, 2018.

[3] S. Dosopoulos and J. F. Lee, "Interior penalty discontinuous Galerkin finite element method for the time-dependent first order Maxwell's equations," *IEEE Transactions on Antennas and Propagation*, vol. 58, no. 12, pp. 4085-4090, 2010.

[4] C. Y. Tian, Y. Shi, and C. H. Liang, "A low-storage discontinuous Galerkin time-domain method," *IEEE Microwave and Wireless Component Letters*, vol. 27, no. 1, pp. 1-3, 2017.

[5] X. L. Li and J. M. Jin, "A comparative study of three finite element based explicit numerical schemes for solving Maxwell's equations," *IEEE Transactions on Antennas and Propagation*, vol. 60, no. 3, pp. 1450-1457, 2012.

[6] A. Taflove and S. C. Hagness. *Computational Electrodynamics: The Finite-Difference Time-Domain Method*. 3rd edition, Artech House, Boston, 2005.

[7] C. Y. Tian, Y. Shi, and C. H. Chan, "Interior

penalty discontinuous Galerkin time domain method based on wave equation for 3D electromagnetic modeling," *IEEE Transactions on Antennas and Propagation*, vol. 65, no. 12, pp. 7174-7184, 2017.

[8] C. Y. Tian, Y. Shi, and C. H. Chan, "An improved vector wave equation-based discontinuous Galerkin time domain method and its hybridization with Maxwell's equation-based discontinuous Galerkin time domain method," *IEEE Transactions on Antennas and Propagation*, vol. 66, no. 11, pp. 6170-6178, 2018.

[9] J. F. Chen and Q. H. Liu, "Discontinuous Galerkin time-domain methods for multiscale electromagnetic simulations: A review," *Proceedings of IEEE*, vol. 101, no. 2, pp. 242-254, 2013.

[10] Y. Shi, C. Y. Tian, and C. H. Liang, "Discontinuous Galerkin time domain method based on marching-on-in-degree scheme," *IEEE Antennas and Wireless Propagation Letters*, vol. 16, pp. 250-253, 2016.

[11] C. Y. Tian, Y. Shi, Z. Q. Liu, and C. H. Liang, "A Laguerre-based time-domain discontinuous Galerkin finite element-boundary integral method," *Microwave and Optical Technology Letters*, vol. 58, no. 11, pp. 2774-2780, 2016.

[12] Y. Shi, C. Y. Tian, Z. Q. Liu, and C. H. Liang, "A new Laguerre-based discontinuous Galerkin time-domain method," *Microwave and Optical Technology Letters*, vol. 59, no. 7, pp. 1499-1503, 2017.

[13] V. Dolean, H. Fahs, and L. Fezoui, "Locally implicit discontinuous Galerkin method for time domain electromagnetics," *Journal of Computational Physics*, vol. 229, no. 2, pp. 512-526, 2009.

[14] S. Piperno, "Symplectic local time-stepping in non-dissipative DGTD methods applied to wave propagation problems," *ESAIM: Mathematical Modelling and Numerical Analysis*, vol. 40, no. 5, pp. 815-841, 2006.

[15] A. Taube, M. Dumbser, C. D. Munz, and R. Schneider, "A high-order discontinuous Galerkin method with time-accurate local time stepping for the Maxwell equations," *International Journal of Numerical Modelling: Electronic Networks, Devices and Fields*, vol. 22, no. 1, pp. 77-103, 2009.

[16] E. Montseny, S. Pernet, X. Ferriéres, and G. Cohen, "Dissipative terms and local time-stepping improvements in a spatial high order discontinuous Galerkin scheme for the time-domain Maxwell's equations," *Journal of Computational Physics*, vol. 227, no. 14, pp. 6795-6820, 2008.

[17] J. Diaz and M. J. Grote, "Energy conserving explicit local time stepping for second-order wave equations," *SIAM Journal on Scientific Computing*, vol. 31, no. 3, pp. 1985-2014, 2009.

[18] J. P. Webb, "Hierarchal vector basis functions of arbitrary order for triangular and tetrahedral finite elements," *IEEE Transactions on Antennas and Propagation*, vol. 47, no. 8, pp. 1244-1253, 1999.

[19] S. D. Gedney and J. A. Roden, "Numerical stability of nonorthogonal FDTD methods," *IEEE Transactions on Antennas and Propagation*, vol. 48, no. 2, pp. 231-239, 2000.

Peng Wang received the B.E. degree in Electronic Science and Technology from the School of Electric Power, North China University of Water Resources and Electric Power, Henan, China, in 2015. He is currently working towards the Ph.D. degree in Electromagnetics and Microwave Technology at Xidian University, Xi'an, China. His research interest convers computational electromagnetics, IH heating technology, electromagnetic compatibility.

Yan Shi received the B.Eng. and Ph.D. degrees in Electromagnetic Fields and Microwave Technology from Xidian University, Xi'an, China, in 2001 and 2005, respectively.

Shi joined the School of Electronic Engineering, Xidian University, in 2005 and was promoted to Full Professor in 2011. From July 2007 to July 2008, he worked at City University of Hong Kong, Hong Kong, China, as a Senior Research Associate. From September 2009 to September 2010, he was a Visiting Postdoctoral Research Associate with the University of Illinois at Urbana-Champaign. From June 2017 to July 2017, he was a Visiting Professor at State Key Laboratory of Millimeter Wave of City University of Hong Kong, Hong Kong, China. He has authors or coauthored over 100 papers in referred journal, a book chapter, and a book. His research interests cover computational electromagnetics, metamaterial, antenna, and electromagnetic compatibility.

Shi received Program for New Century Excellent Talents in University awarded by Ministry of Education of China in 2011, New Scientific and Technological Star of Shaanxi Province awarded by Education Department of Shaanxi Provincial Government in 2013, First Prize of Awards for Scientific Research Results of High Education of Shaanxi Province awarded by Education Department of Shaanxi Provincial Government in 2013, and Second Prize of Awards of Science and Technology awarded by Shaanxi Province Government in 2015. Shi is a Senior Member of IEEE and the Chinese Institute of Electronics (CIE).